Analysis of Distortion in Pulse Modulation Converters for Switching Radio Frequency Power Amplifiers

Vandana Bassoo, Lance Linton and Mike Faulkner

Centre for Telecommunications and Micro-Electronics,

Victoria University, Australia

E-mail: vandana.bassoo@live.vu.edu.au

Abstract

High efficiency linear radio frequency (RF) power amplifiers (PAs) are needed for today's wireless communication systems. Switch mode techniques have the potential for high efficiency but require a pulse drive signal. The generation of pulse width modulated signals and pulse position modulated signals by sigma delta modulators can introduce unwanted spectral components. Third order and image components are the dominant distortions generated in the pulse position modulation circuit. We identify the cause of distortion and mathematically quantify its amplitude and frequency. In a single carrier environment, an increase in offset frequency increases the unwanted spectral components. Calculations, simulations and measurements show that offsets less than 1% of the carrier frequency are required to keep unwanted components 40 dB below the signal level. Simulations and measurements show that the effect on a multi-channel OFDM system is less detrimental. Nonetheless, unacceptable noise increases of up to 20 dB are observed in odd harmonic channels when the transmission is not centered on the nominal carrier frequency.

I. INTRODUCTION

A recent study estimated that by 2013, 80% of the three billion broadband users will be connected through a wireless device [1]. This has to be achieved within the constraints of today's fragmented spectrum, multiple operating standards, and the need for low carbon footprint. Therefore, next generation transmitter architectures need to be bandwidth efficient, power efficient, broadband and flexible. Bandwidth efficient multi-carrier schemes such as orthogonal frequency division multiplexing (OFDM) are normally amplified using conventional linear power amplifiers; however the efficiency is very poor. Switch mode power amplifiers (SMPAs), such as class E amplifiers, are known to be highly efficient but non-linear. Using a pulse train as the drive signal by-passes the linearity issue of SMPAs. The phase and amplitude information is embedded in the edges of the pulse train. Over the years, process technology has improved and it is possible to directly generate the digital drive signals using sigma delta ($\Sigma\Delta$) techniques. All-digital modulators using bandpass or lowpass $\Sigma\Delta$ modulators have been proposed in [2]- [4]. Fig. 1 shows a potential candidate for the future generation wireless transmitters using Class D, E or F SMPAs [1]. The new structure requires a bandpass filter at the output but eliminates the need for most other analog components such as digital to analog converters (DACs), reconstruction filters, the local oscillator and the quadrature modulator. It also provides the possibility of integrating both the digital and microwave sections on to a single chip [5].

Recent $\Sigma\Delta$ solutions have targeted two different problem areas, the first is the reduction of digital processing load, which is necessary for low power operation at microwave frequencies, and the second seeks to improve the efficiency of the SMPA by reducing the switching activity.

---

[1]Class E or F are usually preferred for high carrier frequencies because the parisitics form part of the load network or are resonated out. Class D is suitable for lower operating frequencies [6].

One of the earliest methods uses a fourth-order bandpass $\Sigma\Delta$ clocked at four times the carrier frequency to generate the binary input drive signal for the SMPA [7]. The high clock rate means that the $\Sigma\Delta$ consumes considerable digital power. Researchers in [8]- [9] replaced the bandpass $\Sigma\Delta$ with a two low pass $\Sigma\Delta$ operating at lower clock frequencies. This reduces the $\Sigma\Delta$ sample rate by two. The sample rate reduction in [9] was more aggressive leading to burst mode operation and the digital processing load was further improved. However reducing the $\Sigma\Delta$ sample rate also reduces the signal bandwidth, which was partially compensated for by increasing the effective order of the filter. In the methods described in [8]- [9], switching activity occurs at least once per RF period, even if the input signal is small or absent, leading to an increase in SMPA switching activity.

Two possible techniques that reduce switching activity are the polar $\Sigma\Delta$ [4] and the Cartesian $\Sigma\Delta$ [10]. The polar $\Sigma\Delta$ consists of two lowpass $\Sigma\Delta$s operating on polar representations of the baseband signal, followed by an upconversion block, that performs polar to pulse width modulation (PWM) and pulse position modulation (PPM). The Cartesian $\Sigma\Delta$ uses the same upconversion block but performs the baseband $\Sigma\Delta$ filtering in the Cartesian domain, thus improving the signal to quantisation noise ratio (SQNR) [10]. Both schemes limit the number of pulses to a maximum of one pulse per period (or half period) of the RF carrier. Often there are no switching pulses, when the input signal is small, thus reducing switching loss which is a principal source of power loss in the amplifier. However, in [4], it was mentioned that a number of spurious tones were observed in the output spectrum. The problem was attributed to non-linearities in the modulation process. The authors verified this in [11].

We show that the presence of the spurious tones is due to the PPM process. The significant contribution of this paper is the mathematical analysis which quantifies the distortion. The

dominant distortion products are the third harmonic and the image both of which fold in from other harmonic zones. We validate the results by simulations and measurements. The PPM section is responsible for the phase modulation of the carrier pulse sequence. It inserts or swallows a clock cycle to change the carrier phase (pulse position) by one quantisation level. We show how these quantised phase jumps generate distortion components that affect both the signal amplitude and signal phase. The analysis is performed in a single carrier environment using a single sideband (SSB) test signal. We also use simulation and measurement to show how the distortion can affect a multi-carrier signal. The distortion components can dominate the noise shaping spectrum of the $\Sigma\Delta$ process. We show that the problem can be reduced by increasing the oversampling rate and minimising the signal offset frequency from the centre of the band. Section II describes the architecture of the digital drive block and explains the $\Sigma\Delta$ filter and the 'polar to PWM/PPM' block in detail. Section III intuitively describes the distortion caused by the PPM block. A mathematical analysis of the problem is presented in Section IV. Section V corroborates the theory by simulations and measurements using a SSB test signal. Measurement and simulation results are also provided for a multi-carrier signal. Section VI concludes the work.

II. ARCHITECTURE OF DIGITAL DRIVE BLOCK

Fig. 2 shows the block diagram of the proposed Cartesian $\Sigma\Delta$ which consists of two second-order lowpass $\Sigma\Delta$s (MOD 2) [12], amplitude and phase quantisers and a 'polar to PWM/PPM' block. The 'polar to PWM/PPM' block controls the amplitude of the RF carrier signal by the pulse width and the phase of the RF carrier by the pulse position. These can be updated at a maximum rate of every half cycle of the RF carrier (for the tri-state waveform) or every cycle for the two state version. Lesser update rates are possible in which case a burst of carrier waveforms

is generated for each input sample. The 'polar to PWM/PPM' also oversamples the carrier signal by an oversampling factor, OSR.

A. Sigma Delta Filtering

Synchronous digital circuits mandate the alignment of pulse positions and pulse widths with digital clock edges resulting in the generation of time-based quantisation noise. $\Sigma\Delta$ techniques use oversampling and noise shaping to reduce the noise in the signal band. The noise shaping is determined by the MOD-2 noise transfer function (NTF) which provides increased noise attenuation for frequencies close to DC. The signal transfer function is unity and the NTF is given by

$$NTF = (1 - z^{-1})^2 \tag{1}$$

In operation, the Cartesian signals pass through the $\Sigma\Delta$ filters, after which they are converted to polar $[R, \theta]$ for quantisation in blocks Q_R and Q_θ (Fig. 2). The quantised signals $[\hat{R}, \hat{\theta}]$ are then reconverted to Cartesian before being fed back to the filters [10].

B. Polar to PWM/PPM

The 'polar to PWM/PPM' block is responsible for upconverting the filtered and quantised polar signals to RF using PPM and PWM. The location of the pulse is determined using the quantised phase, $\hat{\theta}$. The phase modulated signal is then fed to a pulse width modulator where the quantised amplitude, $\hat{R}$ is converted to duration as in [4]. The equations from [13] are used to decide the amplitude quantisation levels for the polar quantiser. In this case, the amplitude is quantised into $(\frac{OSR}{2} + 1)$ levels corresponding to pulse widths of $(0, \frac{2}{OSR}, \frac{4}{OSR}, \frac{6}{OSR} \cdots \frac{OSR/2}{OSR})\frac{1}{f_c}$ (f_c = carrier frequency). The phase is quantised into OSR phase increments from zero to 2π.

This quantisation process requires the system digital clock to oversample f_c by a factor of OSR therefore $f_{clk} = OSR f_c$. The pulse edges are confined to the sampling grid with OSR samples per period.

III. PHASE MODULATION TO AMPLITUDE MODULATION DISTORTION

The phase modulation operates by swallowing or stuffing a pulse whenever $\hat{\theta}$ moves from one phase quantisation level to another. The loss or gain of a pulse affects the mark-space ratio which represents the amplitude of the signal. It can thus be deduced that phase modulation (PM) leads to amplitude modulation (AM) distortion. The distortion is more significant when a 'high' pulse is affected. The phenomenon manifests itself in the spectral domain as images and harmonic components when the baseband input signal is a phase ramp or SSB tone in the RF domain.

Fig. 3 shows the pulse extension effect. For illustrative purposes, the repeating pulse train is divided into sections of two periods. Waveform (a) shows the original reference waveform at f_c. At the second period of waveform (b), there is a change in phase. The change in phase is represented by a change in position. In the remaining waveforms, the phase is incremented at every second period to produce a SSB signal at $f_c + f_{ssb}$. A change in phase causes a change in the mark-space ratio between two consecutive pulses. At some stage, the high pulses will join to form a wider high pulse (waveform(i)). The amplitude is no longer one pulsewidth wide.

Since the 'polar to PWM/PPM' block is located outside the $\Sigma\Delta$ loop, the error cannot be corrected by the feedback mechanism. The situation is undesirable since the harmonics are often inband and cannot be filtered out.

IV. Mathematical Analysis of Harmonic Distortion

In this section, we derive expressions for the distortion caused in the 'polar to PWM/PPM block'. In particular, since the distortion is attributed to changes between different phase quantisation levels, the analysis is for a single sideband tone. This signal has constant amplitude and a phase that linearly increases (or decreases) with time to produce an upper (or lower) sideband signal with carrier frequency, $(f_c + f_{ssb})$ or $(f_c - f_{ssb})$ Hz respectively. The phase slope $\frac{d\theta}{dt}$ determines the side band frequency, $f_{ssb} = \frac{1}{2\pi}\frac{d\theta}{dt}$. After quantisation, the linear phase ramp turns into a staircase signal with OSR steps in 2π radians. Therefore, the step size is $\Delta\theta = \frac{2\pi}{OSR}$.

In the digital domain, the PWM operation holds the pulse width constant while the PPM operation slowly increments (or decrements) the pulse position by one clock period, T_{clk}, as each quantised phase level is passed. There are OSR clock periods in each carrier signal period $(T_c = T_{clk}OSR)$. It is the action of switching between two quantised phases that causes the period of the waveform to be extended or shortened by a clock cycle, introducing unwanted amplitude modulation as already illustrated in Fig. 3.

Mathematically, we can consider the output $y(t)$ coming from a switch that selects one oscillator from a bank of OSR oscillators. The k_{th} oscillator has an output signal $s_k(t)$ with quantised phase shift of $k\Delta\theta(k = 0, \ldots, OSR - 1)$, caused by a pulse delay of kT_{clk} seconds as shown in Fig. 4.

$$s_k(t) = s(t + kT_{clk}) \tag{2}$$

All oscillators have the same pulse width VT_{clk} and frequency f_c. Each anti-clockwise rotation of the switch will delay the signal by 2π radians, or reduce the number of transmitted periods by

one. Therefore, the direction and rotational speed (revolutions per second) of the switch equates

to the offset frequency, f_{ssb}. Hence the time for a complete switch revolution is

$$T_{ssb} = \frac{1}{f_{ssb}} \tag{3}$$

and therefore the duration period that each of the OSR oscillators is connected (or gated) to the

output is $T_g = \frac{T_{ssb}}{OSR}$.

Based on the above discussion we can further refine the circuit to that of Fig. 5. A tapped

delay line generates all OSR phases from a single reference oscillator, $s_0(t)$. Each tap has a

delay of T_{clk} seconds. Each oscillator signal is then gated to the output using a multiplier and

gating waveform, $g_k(t)$, which has a period of T_{ssb}, an 'on time' of T_g, and a delay of kT_g. The

output from the k_{th} gate is given by

$$y_k(t) = s_k(t)g_k(t) \tag{4}$$

and the total output is given by

$$y(t) = \sum_{k=0}^{OSR-1} y_k(t) \tag{5}$$

It is now possible to calculate the spectrum of the final output signal. We first calculate the

spectra of the oscillator signal $\tilde{S}_k(f) = F\{s_k(t)\}$ and the gate signal $\tilde{G}_k(f) = F\{g_k(t)\}$.

The operator F is the Fourier transform. Next, we use the fact that multiplication in the time

domain is equivalent to convolution in the frequency domain to get the output spectrum, $\tilde{Y}_k(f)$.

For simplicity, the derivation has been broken down into three distinct sections which is the

derivations of $\tilde{S}_k(f)$, the derivation of $\tilde{G}_k(f)$ and the convolution of $\tilde{S}_k(f)$ with $\tilde{G}_k(f)$ to obtain

a general expression for the output spectral components.

The oscillator signal, $s_0(t)$, is a repeating pulse signal and therefore Fourier Series is used to calculate its spectrum. Its pulse width is given by, VT_{clk}, its pulse amplitude is A, its period is T_c and its spectrum is well known [14].

$$\tilde{S}_0(f) = \sum_{n=-\infty}^{\infty} S_0(n)\delta(f - nf_c) \tag{6}$$

where

$$S_0(n) = \frac{AVT_{clk}}{T_c}\text{Sinc}\left(\frac{nVT_{clk}}{T_c}\right) \tag{7}$$

Since $(T_c = T_{clk}OSR)$, $S_0(n)$ can be re-written as

$$S_0(n) = \frac{AV}{OSR}\text{Sinc}\left(\frac{nV}{OSR}\right) \tag{8}$$

This is a series of delta functions at the harmonics of f_c and with amplitude controlled by the Sinc function which gradually decays in an oscillatory fashion as $|n|$ increases. In the model a change in phase is represented by a change (delay or advance) in pulse position, so the time shifting property of the Fourier Transform is invoked. Hence:

$$\tilde{S}_k(f) = \sum_{n=-\infty}^{\infty} S_k(n)\delta(f - nf_c) \tag{9}$$

$$S_k(n) = \frac{AVT_{clk}}{T_c}\text{Sinc}\left(\frac{nVT_{clk}}{T_c}\right)e^{\frac{j2\pi nk}{OSR}} \tag{10}$$

and $k = 0, 1, \ldots, (OSR - 1)$.

$$S_k(n) = S_0(n)e^{\frac{j2\pi nk}{OSR}} \tag{11}$$

The gate signal, $g_k(t)$ is a repetitive pulse train which has a period of T_{ssb}. The 'on period' of this pulse train is given by $\frac{T_{ssb}}{OSR}$.

$$\tilde{G}_0(f) = \sum_{m=-\infty}^{\infty} G_0(m)\delta(f - mf_{ssb}) \tag{12}$$

where

$$G_0(m) = \frac{1}{OSR}\text{Sinc}\left(\frac{m}{OSR}\right) \tag{13}$$

The delayed version $G_k(f)$ by KT_{clk} is given by

$$\tilde{G}_k(f) = \sum_{m=-\infty}^{\infty} G_k(m)\delta(f - mf_{ssb}) \tag{14}$$

$$G_k(m) = G_0(m)e^{\frac{j2\pi mk}{OSR}} \tag{15}$$

The convolution of $\tilde{S}_k(f)$ and $\tilde{G}_k(f)$ gives $\tilde{Y}_k(f)$.

$$\tilde{Y}_k(f) = \sum_{n=-\infty}^{\infty} S_k(n)\delta(f - nf_c) \otimes \sum_{m=-\infty}^{\infty} G_k(m)\delta(f - mf_{ssb}) \tag{16}$$

Convolution of delta functions effectively imprints the G spectrum on each harmonic of f_c. After substituting for $S_k(n)$ (equation(11)) and $G_k(m)$ (equation(15))

$$\tilde{Y}_k(f) = \sum_{n=-\infty}^{\infty}\sum_{m=-\infty}^{\infty} S_0(n)G_0(m)e^{\frac{j2\pi(m+n)k}{OSR}} \times \delta(f - nf_c - mf_{ssb}) \tag{17}$$

The total $\tilde{Y}(f)$ spectrum is the sum of each gated phase spectrum, $\tilde{Y}_k(f)$

$$\tilde{Y}(f) = \sum_{K=0}^{OSR-1} \tilde{Y}_k(f) \tag{18}$$

$$= \sum_{K=0}^{OSR-1} \sum_{n=-\infty}^{\infty} \sum_{m=-\infty}^{\infty} S_0(n)G_0(m)e^{\frac{j2\pi(m+n)k}{OSR}} \times \delta(f - nf_c - mf_{ssb}) \tag{19}$$

The above equation can be simplified if the summation of k is implemented first. It can be seen that a harmonic is produced only when $m + n = \text{integer} \times (OSR)$. The exponential term sums to zero for all other combinations of m and n, when $m = i(OSR) - n$ and i is any integer, the output becomes

$$\tilde{Y}(f) = OSR \sum_{n=-\infty}^{\infty} \sum_{m=-\infty}^{\infty} S_0(n)G_0(m)\delta(f - nf_c - mf_{ssb}) \tag{20}$$

The amplitude of the harmonic is given by $S_0(n)G_0(m)OSR$ and the delta function gives its position in the spectrum. Sometimes many harmonics have the same frequency and their contributions must be summed. However, those with large m values will have small amplitudes because of the decay of the Sinc function. For this reason, spectra from the closest carrier frequency harmonics (small n) need only be considered.

As an example we set $OSR = 16$ and $V = 2$ and $f_{ssb} = \frac{f_c}{16}$. The spectrum consists of a spur at DC ($m = 0, n = 0$) of amplitude $\frac{AVT_{clk}}{T_c} = \frac{2}{OSR}$. The desired SSB signal occurs about the first harmonic zone with $n = 1, i = 0$ and $m = -1$ giving the lower side band at $f = f_c - f_{ssb}$. The undesired second harmonic (of f_{ssb}) occurring at $f = f_c - 2f_{ssb}$ folds back from the second harmonic zone ($n = 2, i = -1$ and $m = -16 - 2$). The third harmonic at $f = f_c - 3f_{ssb}$ folds back from the third harmonic zone ($n = 3, i = -2$ and $m = -32 - 3$ and the signal image at

$f_c + f_{ssb}$ comes from the negative harmonic zone at $-f_c(n = -1, i = 2, m = 32 + 1)$.

The current formulation is for a single ended (two state, 0 and A) signal only. The above analysis can be extended to include the tri-state signal of Fig. 2 by modifying the expression for $s_k(t)$ in equation (2) to

$$s_k(t) = s(t + kT_{clk}) - s\left(t + kT_{clk} - \frac{T_c}{2}\right) \tag{21}$$

The spectrum of this signal can be obtained by the normal time shifting property. The result of adding this term is to double the signal level for all odd harmonics of f_c and to zero all even harmonics of f_c. This effectively eliminates the folded spectrum from the even harmonic zones (n, even) which include the DC term and the even harmonics of f_{ssb} as shown in Fig 6.

V. SIMULATION AND MEASUREMENT RESULTS

In this section, the phenomenon is simulated and quantified by using two test signals, a SSB tone and a multi-carrier signal such as OFDM. All simulations were performed in Matlab®. Measurements using SSB and OFDM as input signals were performed. The experimental setup comprised of the $Tektronix$® data timing generator connected to a spectrum analyser.

A. Analysis in Single Carrier Environment

Here, the test signal is a SSB tone, offset by 40 MHz from the carrier frequency. Fig. 6 shows the spectrum plot of the SSB signal obtained at the output of the 'polar to PWM/PPM' block. The position of the reference carrier is drawn for illustrative purposes. The signal can be observed (40 MHz offset from the carrier). The image and the third harmonic can be seen rising far above the noise floor. It can also be noted that the average noise floor is much lower

compared to the similar spectrum plot in [11] where the $\Sigma\Delta$ filtering was performed on polar signals.

Fig. 7 shows a plot of simulated, calculated and measured values of the image, the second and the third harmonic against varying offset frequency, f_{ssb}. The OSR is kept to 32 and f_{ssb} varied up to $\frac{f_c}{16}$. The higher the value of f_{ssb}, the larger the distortion, because the switching transients occur more often. A doubling of f_{ssb} increases the distortion products by approximately 6 dB. The size of the second harmonic oscillates between a lower and an upper limit depending on the ratio of f_c and f_{ssb}. An even ratio produces the upper limit while an odd ratio produces the lower boundary (Fig. 7). The second harmonic curve does not exist for the three state signal (Fig 2), but does if only a two state signal is used. The close proximity to the desired signal and the dominant nature of the second order distortion justifies the additional expense associated with the implementation of a bridge amplifier structure to make the three state signal. The dotted lines on Fig. 7 show the evaluated results from equation (20). The markers on Fig. 7 show the measured results. The simulated values were obtained by applying a constant amplitude signal with varying phase to the 'polar to PWM/PPM' block of Fig. 2. Close agreement between the simulated, calculated and measured values is observed. A measured spectrum plot showing the second harmonic, third harmonic and image is presented in Fig. 8.

B. Analysis in Multi-Carrier Environment

A quadrature phase shift keying (QPSK) modulated OFDM input signal with a worst case peak to average power level of 8 dB was used to test the architecture. The OFDM bandwidth (B_{ofdm}) was set at $\frac{f_c}{64}$ equivalent to a B_{ofdm} of 16 MHz (similar to 802.11g) with f_c=1024 MHz. There is a guard band between adjacent channels of $0.25B_{ofdm}$. The signal was shifted one channel to the right to examine the resultant spectral images. The adjacent channel powers

(ACPs) which is defined as the noise power in the adjacent channel divided by the signal power were calculated. The noise power includes quantisation noise as well as distortions arising from PPM.

Fig. 9 shows a simulation plot of the input power (dB) against the ACP (dB) for the six adjacent channels. The optimum input power is -7 dB, just before the onset of signal overload in the $\Sigma\Delta$ converters. It can be observed that channel 3 has the highest noise as it represents the third harmonic. Channel -1 represents the image and has the second highest noise. Channel 0 has lower noise than channel 2 as channel 0 is centered at f_c. The maximum attenuation of quantisation noise occurs around that region as the NTF of the $\Sigma\Delta$ operates from f_c.

Table 1 helps to further illustrate the effect of offset on ACP. It gives a comparison of ACP values for Cartesian $\Sigma\Delta$ with offset and without offset. The values were obtained at an input power of -7 dB. Shifting the signal to channel 1 increases the noise in all channels. Those channels containing the odd harmonics are particularly affected with noise increases of 20 dB (channel 3), 15 dB (channel -1) and 13 dB (channel -3). A reduction in the noise can be seen in the channel 0 as the NTF of the $\Sigma\Delta$ operates from f_c. A higher oversampling rate will be required to meet the WLAN standard (ACP $<$-40 dB) or f_c can be increased to reduce the relative offset frequency. Increasing f_c by 2.5 will reduce the main interference channels by 8 dB which should then meet the WLAN specification. Alternatively, the WLAN standard is easily met if the signal is not shifted to the adjacent channels. In fact, in this case the OSR can even be reduced from 64 to a value as low as eight [15].

Spectrum measurement was performed using multi-carrier signals to further substantiate our findings. An OFDM signal with an input power of -7 dB was programmed into the data timing generator. A 3-level waveform (Fig. 2) was used as it suppresses the even harmonics. Fig. 10

Channels No.	-3	-2	-1	0	1	2	3
ACP (dB) no offset	-57	-59	-54	Data	-55	-59	-57
ACP(dB) 1 channel offset	-44	-50	-39	-69	Data	-47	-37

TABLE I
ACP FOR CARTESIAN $\Sigma\Delta$ WITH OFFSET AND WITHOUT OFFSET. CHANNEL 0 IS CENTERED ON f_c. OSR=64.

shows the spectrum analyser display for a pulse waveform with an OSR of 64. The images and harmonics which arise as a result of the offset are clearly visible. The measured result agrees with simulations, except for some small artifacts in channel 0 of the measured signal. The discrepancies can be attributed to the limitation in the slew rate capability of the experimental setup and the mismatches in the positive and negative going waveforms. The negative slope of the signal image in channel -1 can be explained by the fact that OFDM is made up of many individual tones. As the offset between the tones and f_c increases, the size of the distortions of each tone image increases as shown by Fig. 7. The third harmonic and the image of the third harmonic are smeared over a number of channels, but most of the energy is concentrated within channel 3 and -3 respectively. It is quite evident that the inband noise is dominated by the distortions as a result of the 'polar to PWM/PPM' conversion whereas the out-of-band noise is dictated by the noise shaping effect of the $\Sigma\Delta$. This is illustrated by the gradual rise in the noise level at the extremities of the spectrum as shown by the wide span view (Fig. 10 insert).

VI. CONCLUSION

This paper has identified a problem occurring when quantised phase shifts are converted to pulse positions in a digital 'polar to PWM/PPM' block. The quantisation in phase causes significant distortion. This paper proposes a mathematical solution to predict the amplitude

and frequency of the distortion products. It also demonstrates that the distortion increases with increasing offset frequency by almost 6 dB/octave. The offset frequency must be less that 1% of f_c to guarantee distortions less than -40 dB for narrowband signals (Fig. 7). Increasing the OSR helps to alleviate the problem (-6 dB/octave), but it also reduces the maximum carrier frequency. The use of higher order $\Sigma\Delta$ structures will not be effective either, since the PPM distortion dominates the in-band spectrum. (Note: The 'polar to PWM/PPM' block is not enclosed in the $\Sigma\Delta$ feedback loop.) A potential solution is to avoid quantising the phase by using analog techniques [16] but this removes many of the advantages of this all-digital structure.

In a multi-carrier environment, measurements and simulations show that it is best to avoid changing channels by offsetting the carrier frequency because of increasing adjacent channel interference in odd harmonics channels. Some of the distortions can be cancelled by using a bridge amplifier structure to give a three-level signal. In order to meet the WLAN standard, it is preferable to accommodate any channel change by altering the system clock frequency, f_{clk}, in which case WLAN specifications can be met with a much reduced OSR.

References

[1] www.ericsson.com/technology/whitepapers/sustainableenergy.pdf, accessed November 2009

[2] Stapleton, S.P.: 'Class S Power Amplifiers for RF Systems (using Bandpass Delta-Sigma Modulators)', Agilent EEsof Design Seminar, Prod No. N3508A.

[3] Keyzer, J., Hinrichs, J., Metzger, A., Iwamoto, M., Galton, I., Asbeck, P.: 'Digital Generation of RF signals for Wireless Communications with Band-Pass Delta Sigma Modulation', Proc. 2001 IEEE MTT-S Int. Microwave Symp. Dig., May 2001, pp 2127-2130.

[4] Keyzer, J., Uang, R., Sugiyama, Y., Iwamoto, M., Galton, I., Asbeck, P.M.: 'Generation of RF Pulsewidth Modulated Microwave Signals using Delta-Sigma Modulation', Proc. 2002 IEEE MTT-S Int. Microwave Symp. Dig., June 2002, pp. 397-400.

[5] Asbeck, P., Galton, I., Keh-Chung Wang, Jensen, J.F., Oki, A.K., Chang, C.T.M.:'Digital Signal Processing - Up to Microwave Frequencies', IEEE Trans. Microwave Theory and Techn., March 2002, 50,(30), pp 900-909.

[6] Raab, F.H., Asbeck, P., Cripps, S., Kenington, P.B., Popovic, Z.B., Pothecary, N., Sevic, J.F., Sokal, N.O.:'Power amplifiers and transmitters for RF and microwave', IEEE Trans. Microwave Theory Tech., March 2002, 50,(3), pp 814-826.

[7] Jayaraman, A., Chen, P.F., Hanington, G., Larson, L., Asbeck, P.: 'Generation of RF Pulsewidth Modulated Microwave Signals using Delta-Sigma Modulation', IEEE Microwave and Wireless Components Letters., 1998, 8, (3), pp 121-123.

[8] Frappe, A., Flament, A., Stefanelli, B., Cathelin, A., Kaiser, A.:'All-digital RF signal generation for software defined radio', Proc. 4th European Conference on Circuits and Systems for Communications, July 2008, pp 236-239

[9] Helaoui, M., Hatami, S., Negra, R., and Ghannouchi, F.:'A novel architecture of Delta-Sigma Modulator Enabling All-Digital Multiband Multistandard RF Transmitters Design', IEEE Trans. Circuits and Systems II., 2008, 55,(11), pp 1129-1133

[10] Bassoo, V., and Faulkner, M.: 'Sigma Delta Digital Drive Signals for Switchmode Power Amplifiers', Electronic Letters, 2008, 44,(22), pp 1299-1300.

[11] Bassoo, V., Mustafa, A., and Faulkner, M.: 'Distortion Arising from Polar to PWM/PPM Conversion in an All Digital Upconverter for Switching RF Power Amplifier'. Proc. IEEE IMS Int. Microwave Symposium, Boston, USA, June 2009, pp. 1533-1536.

[12] Schreier, R., and Temes, G.C.: 'Understanding Delta-Sigma Data Converters' (Wiley-IEEE Press, 2004).

[13] Wagh, P., and Midya, P.: 'High Efficiency Switched-Mode RF Power Amplifier'. Proc. 42nd Midwest Symposium on Circuits and Systems, 1999, Vol. 2, pp. 1044-1047.

[14] Ifeachor, E., and Jervis, P.: 'Digital Signal Processing : A practical Approach' (Prentice Hall, 2002)

[15] Bassoo, V., Tom, K., Mustafa, A.K., Cijvat, E., Sjoland, H., and Faulkner, M.: 'A Potential Transmitter Architecture for Future Generation Green Wireless Base Station', EURASIP Journal on Wireless Communication and Networking, 2009, Article ID 821846, 8 pages, 2009. doi:10.1155/2009/821846

[16] Jeong, J., and Wang, E.Y.: 'A Polar Delta-Sigma Modulation Scheme for High Efficiency Wireless Transmitters'. Proc. IEEE IMS Int. Microwave Symposium, Honolulu, USA, June 2007, pp. 73-76.
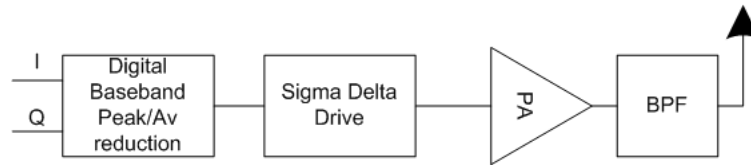
Fig. 1. Proposed transmitter architecture

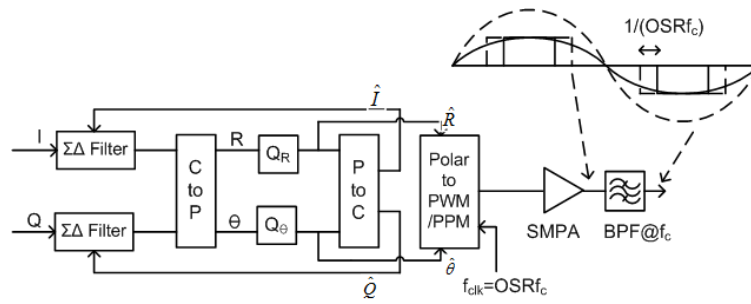
Fig. 2. Block diagram of Cartesian $\Sigma\Delta$. The $\Sigma\Delta$ filter operates at a sample rate of $f_s \leq f_c$
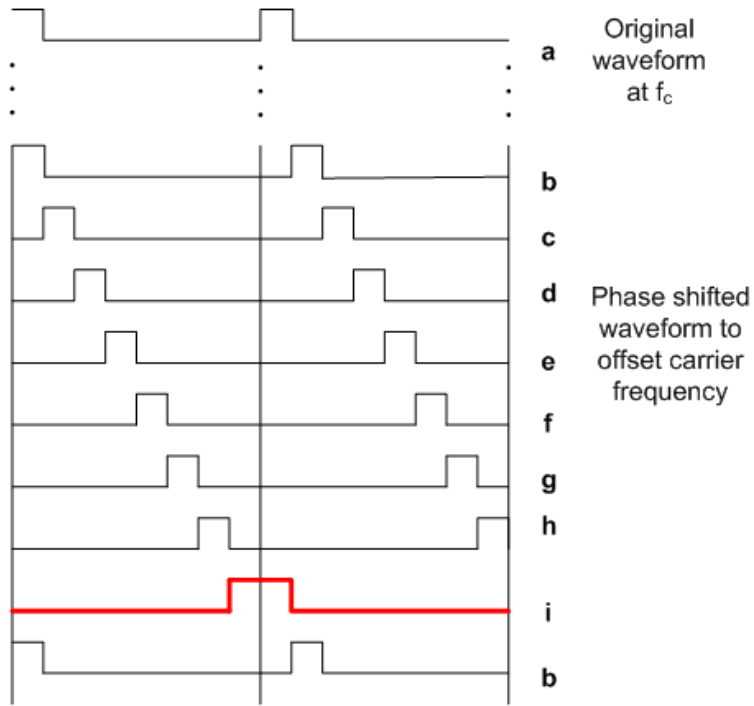
Fig. 3. Illustrating the pulse stuffing effect required to effect a change in phase of the RF signal. (a) carrier reference signal, (b) to (i) signal with phase advanced transient. Here the phase is quantised into 8 increments.
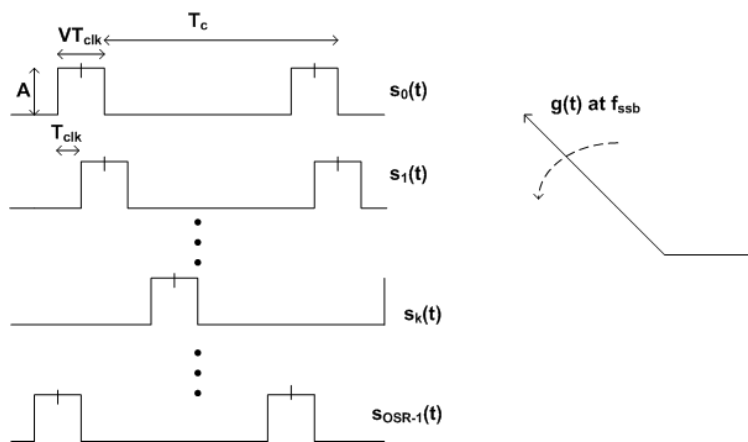

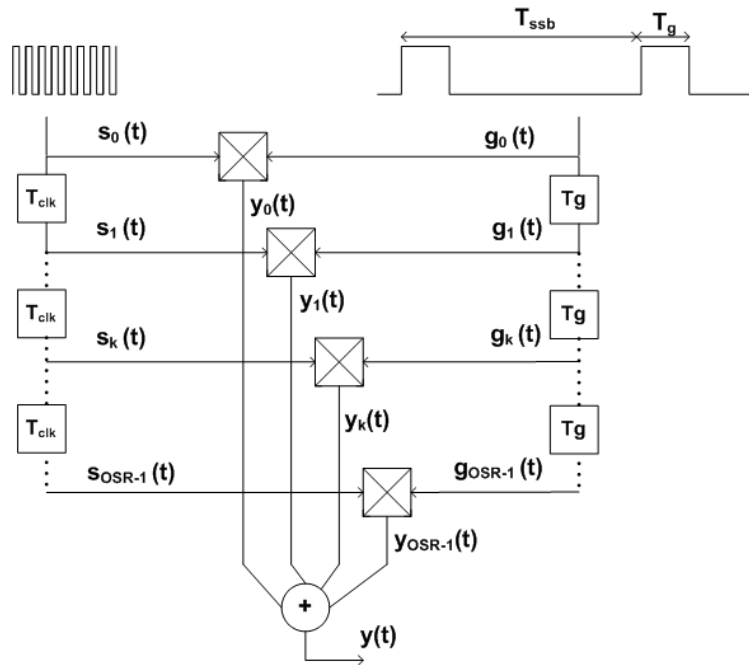Fig. 4. SSB generation from a bank of phase shifted oscillators

Fig. 5. SSB generation for mathematical analysis
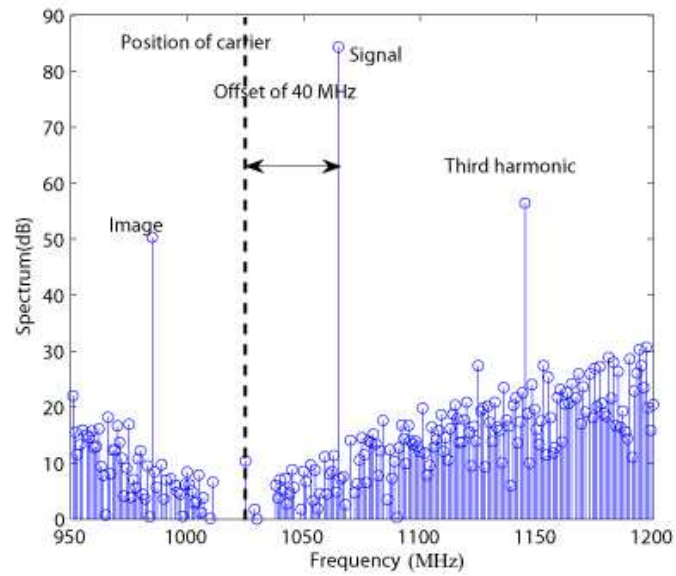
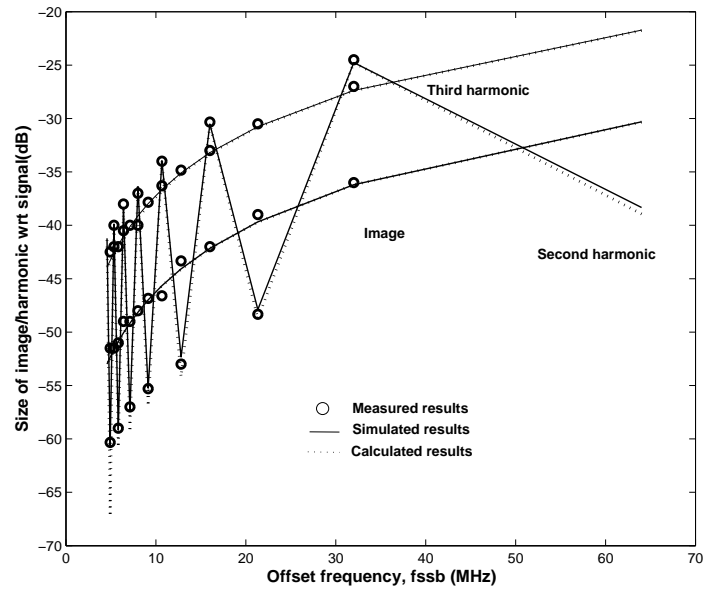Fig. 6. SSB output spectrum from a Cartesian $\Sigma\Delta$. The distortions are from the PWM/PPM image and third harmonic.(f_c=1024 MHz and f_{ssb}= 40 MHz)

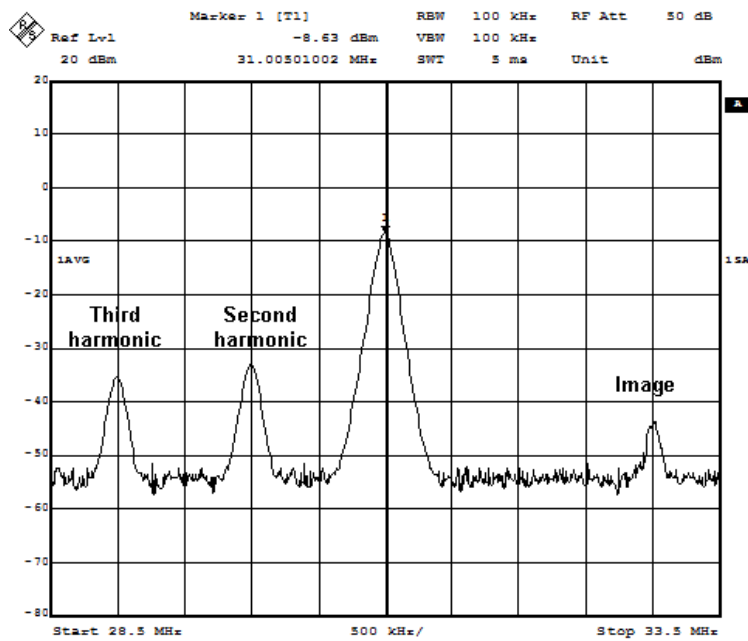Fig. 7. SSB harmonics and image. Amplitude (relative to signals) vs. f_{ssb}. (OSR=32, f_c=1024 MHz)

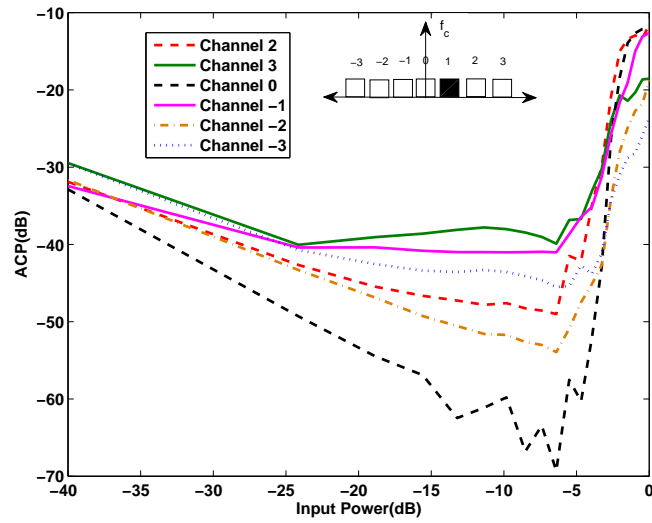Fig. 8. Spectrum measurement. f_c=1024 MHz, f_{ssb}=32 MHz, OSR=32

Fig. 9. ACP in adjacent channels vs. input power. The signal is in channel 1. OSR=64.
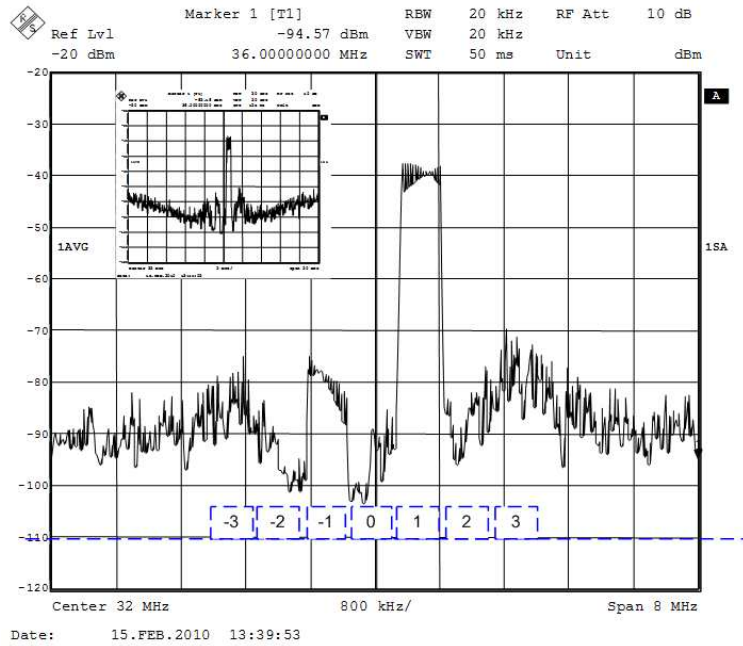

Fig. 10. Spectrum measurements. f_c=32 MHz and an OSR=64. The channels are shown. The insert displays a wider spectrum view of the same signal.